Q. J. R. Meteorol. Soc. (2005), **131**, pp. 1–999 doi: 10.1256/qj.yy.n

A Global Eta Model on Quasi-uniform Grids

By Hai Zhang[1] and Miodrag Rančić[2*]

Joint Center for Earth Systems Technology, University of Maryland Baltimore County, USA

Summary

Application of the quasi-uniform grids in global models of the atmosphere is an attempt to increase the computational efficiency by a more cost effective exploitation of the computing infrastructure. This paper describes the development of a global version of NCEP's regional, step-coordinate, Eta model on two quasi-uniform girds: cubic and octagonal. The governing equations are expressed in a general curvilinear form, so that the cubic and the octagonal version of the model share the same code in spite of different mapping of the computational domain.

The dynamical core of the derived global Eta model is successfully tested in the benchmark test of Held and Suarez. The model with the step-wise formulation of the terrain and full physics is integrated in a series of tests with real data, and the results are compared both with the analysis and the results of the regional Eta model.

Keywords: quasi-uniform grids global model Eta

1. Introduction

The objective of this paper is to investigate application of the *quasi-uniform grids* for discretization of the governing equations on the sphere, as a solution to the *polar problem* of the general circulation models of the atmosphere.

The polar problem is a by-product of the standard longitude-latitude grid and has several aspects. The singular character of geographical poles breaks the pattern of discretization of atmospheric equations on the sphere and complicates preservation of various integral constraints of the continuous equations within their finite-difference approximations. The application of polar Fourier filtering (Arakawa and Lamb 1977), which is a traditional response to the strong increase of resolution in the latitudinal direction close to poles due to the convergence of the meridians, is an effective measure for increasing the minimum time-step, but raises many concerns. The most serious of them is a notion that the polar filtering represents a typical example of an inefficient exploitation of the computing infrastructure. The areas around poles are first excessively resolved - wasting memory, and then, through Fourier filtering of the fast modes, the effect of this resolving is removed - wasting the computing time as well. The situation is especially serious in the environment of contemporary distributed memory computers, where a spatial selectiveness of the polar filtering affects the computational balance, causing additional downgrades of the performance.

With the quasi-uniform grids we evade the polar problem, by replacing the longitude-latitude grid with a mesh of equal (or approximately equal) grid elements. Such a "quasi-uniform" gridding of the sphere may involve the *overlapping* grids (e.g., Phillips 1959; Browning *et al.* 1989) or a *continuous* mapping (e.g., Sadourny *et al.* 1968; Williamson 1970). In this paper, we consider only the quasi-uniform *square* grids, which have the rectangular base elements, as opposed to the various geodesic grids with the *triangular* structure of the basic grid elements (e.g., Ringler and Randall 2002).

Sadourny (1972) suggested first such, a 'cubic', grid for the application in the general circulation models of the atmosphere. Sadourny's cubic grid is derived by

* Corresponding author: JCET, Academic IV, 1000 Hilltop Circle, Baltimore, MD 21250, USA.
e-mail: mrancic@umbc.edu

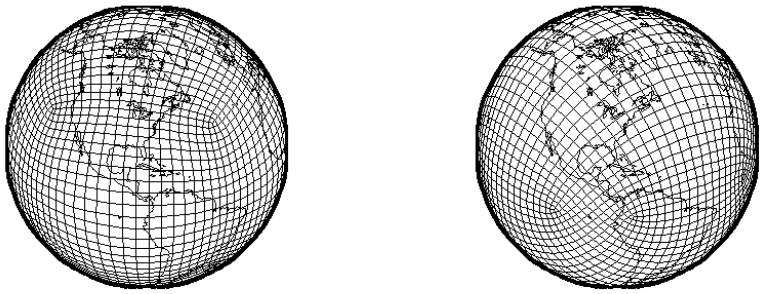

Figure 1. Quasi-uniform grids: cubic (left) and octagonal (right).

a gnomonic projection of the cube to the circumscribed sphere. In the last decade or so, the distributed memory computers brought once again the application of the rectangular quasi-uniform grids in the centre of attention. Rančić *et al.* (1996) suggested a "conformal" cubic grid as an elegant solution to the problem of an angular discontinuity of the coordinate lines across the edges of the Sadourny's gnomonic cube. Ronchi *et al.* (1996) presented an effective overlapping method on the cubic grid. Purser and Rančić (1997) expanded the set of quasi-uniform grids by introducing an octagonal grid (or more precisely, the whole series of octagonal grids with an increasing level of complexity), on which the singular points are arranged along the equator. Within a further refinement of the grid-generation technique, Purser and Rančić (1998) enhanced the regularity of the grid-point distribution on both cubic and octagonal grids.

The most striking features of these grids are the application of a general curvilinear formalism for discretization and the capability to equally distribute the computational load between the processing elements. One can apply exactly the same code on the cubic grid, all octagonal grids, as well as on any other continuous and, with small modifications, overlapping quasi-uniform grids with the rectangular base elements. Thus, a single unifying model can use any of these grids, with an appropriate choice of communications among the processors that corresponds to the particular grid topology.

In the last couple of years, several authors accepted quasi-uniform square grids as the grid-geometry of choice for the global ocean and/or atmospheric models (e.g., McGregor 1996; McGregor and Dix 2001; Tsugawa *et al.* 2003; Adcroft *et al.* 2004). In this paper, instead of developing a new global model on the quasi-uniform grid, we combine the technique of quasi-uniform gridding of the sphere with the numerical infrastructure of the regional Eta model, in order to create a global (or rather, a *globalized*) version of the Eta model. A global model developed on the quasi-uniform grid has an inclusive design and we refer here to the global Eta model as a *Global Eta Framework* (GEF). In this paper, the only grids included in this modelling framework are the cubic and the basic octagonal grid (Figure 1).

The NCEP's (National Centers for Environmental Prediction) regional Eta model is a Eulerian grid-point model, whose dynamics is developed following the Arakawa principles of integral conservation and of acting on the cause of

a numerical problem rather than on its consequences. The early version of the model has been developed at a 'Belgrade Numerical School', in former Yugoslavia, created and led by Dr. Fedor Mesinger and Dr. Zaviša Janjić, the principle authors of the model. Later developments at NCEP are described, for example, in Mesinger *et al.* (1988), Janjić (1990; 1994), Black (1994), and Mesinger *et al.* (2002). The distinguished features of the model are a unique, step-wise treatment of the lower boundary (Mesinger 1984), and a comprehensive physical package (Janjić 1990; 1994), with inclusion of the land-surface processes (e.g., Chen *et al.* 1997; Ek *et al.* 2003).

A global version of the regional model, beside a broader spatial coverage, is also expected to perform better over the domain covered by the regional model. A poor resolution and inadequate treatment of the lateral boundary conditions are generally considered to be one of the major sources of errors in the limited-area models (e.g., Warner *et al.* 1997). A global model eliminates the lateral boundary problem and should provide longer and more accurate weather forecast and climate simulations over a specific region of interest.

Section 2 presents the governing equations applied on the quasi-uniform grids. Section 3 describes numerical methods used to discretize the continuous equations. In section 4, we demonstrate the results of test integrations, which include the Held and Suarez (1994) benchmark test for comparison of dry cores of atmospheric models, and the first experiments with real data and full physics. We provide concluding comments in section 5.

2. Governing equations

The hydrostatic vertical *eta* (η) coordinate (Mesinger 1984), is defined as

$$\eta = \frac{p - p_T}{p_S - p_T}\eta_S \,, \tag{1}$$

where

$$\eta_S = \frac{p_{rf}(z_S) - p_T}{p_{rf}(0) - p_T} \,. \tag{2}$$

The subscripts S and T stand for the surface and the top of model's atmosphere. $p_{rf}(z)$ is a suitably defined reference pressure expressed as a function of height. z_S denotes predefined reference heights of the terrain which may take only discrete values. With such a step-wise formulation of the lower boundary, unlike with the customary terrain following used in the σ system of Phillips (1957), the coordinate surfaces remain nearly horizontal, which eliminates errors of the pressure gradient force close to the steep terrain (Mesinger and Janjić 1985). The blocking effect of the step-terrain enforces the component of the flow around the terrain, which is underestimated in the σ system and is believed to contribute to a more realistic precipitation forecast (e.g., Mesinger 1996).

The coordinate lines on the cubic and the octagonal grids are strictly conformal far from the singular points. Close to the singularities, the conformality constraint is broken, and the coordinates become curvilinear. The smoothed versions of these grids introduced in Purser and Rančić (1998), have the larger minimum grid distance, but the area where the orthogonality does not apply is also broader. Therefore, in order to describe correctly flow on the quasi-uniform grids, the governing equations need to be expressed in terms of a general curvilinear coordinate system.

Let (x, y) define a general curvilinear coordinates on the sphere, and let $\mathbf{a_1}$ and $\mathbf{a_2}$ be the base vectors of the coordinate transformation in the direction of x and y axis, respectively.

The metric tensor of transformation, $\mathbf{G}$, is defined as

$$\mathbf{G} = G_{ij} = \mathbf{a_i} \cdot \mathbf{a_j} \,, \qquad i, j = 1, 2 \,. \tag{3}$$

G is the Jacobian of transformation, defined as $G = [det(G_{ij})]^{\frac{1}{2}}$.

The covariant winds in this system are defined by:

$$\begin{aligned} u &= \mathbf{V} \cdot \mathbf{a_1} \,, \\ v &= \mathbf{V} \cdot \mathbf{a_2} \,. \end{aligned} \tag{4}$$

The contravariant winds are related to the covariant winds via

$$\begin{pmatrix} \tilde{u} \\ \tilde{v} \end{pmatrix} = \mathbf{G^{-1}} \begin{pmatrix} u \\ v \end{pmatrix} . \tag{5}$$

The relative vorticity is given by

$$\zeta = \frac{1}{G}\left(\frac{\partial v}{\partial x} - \frac{\partial u}{\partial y}\right) , \tag{6}$$

and the kinetic energy by

$$K = \frac{1}{2}(\tilde{u}u + \tilde{v}v) \,. \tag{7}$$

Further details on application of the general curvilinear coordinate system in the context of atmospheric primitive equations can be found in Sadourny (1972) and Rančić *et al.* (1996).

The momentum, the thermodynamic and the continuity equations are respectively:

$$\frac{\partial u}{\partial t} = (\zeta + f)G\tilde{v} - \frac{\partial K}{\partial x} - \dot{\eta}\frac{\partial u}{\partial \eta} - \frac{\partial \Phi}{\partial x} - \frac{RT_v}{p}\frac{\partial p}{\partial x} + F_u \,, \tag{8}$$

$$\frac{\partial v}{\partial t} = -(\zeta + f)G\tilde{u} - \frac{\partial K}{\partial y} - \dot{\eta}\frac{\partial v}{\partial \eta} - \frac{\partial \Phi}{\partial y} - \frac{RT_v}{p}\frac{\partial p}{\partial y} + F_v \,, \tag{9}$$

$$\frac{\partial T}{\partial t} = -\left(\tilde{u}\frac{\partial T}{\partial x} + \tilde{v}\frac{\partial T}{\partial y}\right) - \dot{\eta}\frac{\partial T}{\partial \eta} + \frac{1}{c_p}\frac{RT_v}{p}\omega + \frac{Q}{c_p} \,, \tag{10}$$

$$\frac{\partial}{\partial \eta}\left(\frac{\partial p}{\partial t}\right) = -\frac{1}{G}\left[\frac{\partial}{\partial x}(\tilde{u}Gm) + \frac{\partial}{\partial y}(\tilde{v}Gm)\right] - \frac{\partial}{\partial \eta}(\dot{\eta}m) \,. \tag{11}$$

The hydrostatic equation is written as:

$$\frac{\partial \Phi}{\partial \eta} = -\frac{RT_v}{p}m \,. \tag{12}$$

Here, the symbols have their usual meanings. The momentum equation is written in a vector invariant form, which conveniently encapsulates the curvilinear terms. The mass m is defined as

$$m = \frac{\partial p}{\partial \eta} \,. \tag{13}$$

The vertical velocity $\dot{\eta}$ is derived from the continuity equation (11)

$$\dot{\eta}\frac{\partial p}{\partial \eta} = -\frac{\partial p}{\partial t} - \int_0^{\eta} \frac{1}{G}\left[\frac{\partial}{\partial x}(\tilde{u}Gm) + \frac{\partial}{\partial y}(\tilde{v}Gm)\right] d\eta \,. \tag{14}$$

Similarly, the time tendency of surface pressure is computed by integrating the horizontal divergence over all layers:

$$\frac{\partial p_S}{\partial t} = -\int_0^{\eta_S} \frac{1}{G}\left[\frac{\partial}{\partial x}(\tilde{u}Gm) + \frac{\partial}{\partial y}(\tilde{v}Gm)\right] d\eta \,. \tag{15}$$

In addition, the transport of a number of atmospheric scalar variables (specific humidity, cloud water, turbulent kinetic energy, etc.) is described by:

$$\frac{\partial q}{\partial t} = -\left(\tilde{u}\frac{\partial q}{\partial x} + \tilde{v}\frac{\partial q}{\partial y}\right) - \dot{\eta}\frac{\partial q}{\partial \eta} + Q_s \,, \tag{16}$$

where Q_s are various source and sink terms.

3. Numerical Methods

In this section, we describe the numerical infrastructure used in the Global Eta Framework. Most of the schemes are simply taken from the regional Eta model. However, some of the numerical techniques require special modifications, or, in some cases, an adequate replacement, in the general curvilinear system.

(*a*) *Horizontal and vertical arrangement of variables*

The cubic and octagonal quasi-uniform grids (Figure 1) consist respectively, of 6, and of 14 (or alternatively, 28, if placed diagonally) basic topological elements. On the cubic grid, these basic grid elements are identical and coincide with the faces of the cube. On the octagonal grid, they have equal number of grid points but cover slightly different areas. More isotropic versions of the octagonal grid are also available (see Purser and Rančić 1997), but they are not considered in this paper. In implementations on the parallel computers, each basic topological element is allocated to its own processor, so that the amount of data load and computation (at least in the portion of the code which describes the atmospheric dynamics) is equally distributed among processors. Because of the general curvilinear formalism, the only difference in computation on the cubic and the octagonal grid is in definition of communications between the processing elements. The basic grid elements can be further divided into 2^2, 3^2, 4^2, ..., smaller pieces (tiles) depending on the number of available processors and required resolution.

The semi-staggered B-grid, following Arakawa notation (Figure 2), is used for horizontal staggering of model variables. The B-grid substantially simplifies indexing in comparison to the E-grid, which is used in the regional Eta model. Because the B- and the E-grid are rotated versions of each other by an angle of 45°, we are still able to use the efficient E-grid numerical schemes on the B-grid, assuming that the main coordinate lines (x, y) are on the B-grid aligned

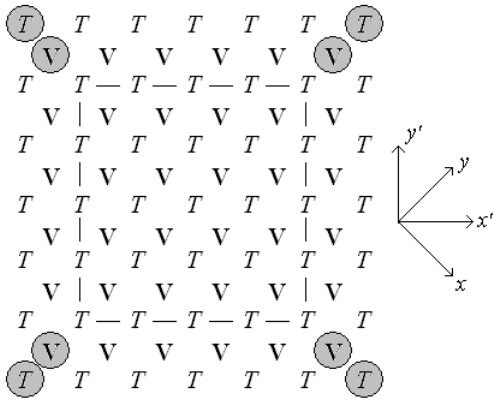

Figure 2. Arakawa B-grid arrangement of variables on a tile of a quasi-uniform grid. T represent scalar points and $\mathbf{V}$ vector points. If the tile is associated with the corner singularity, then the circled points are located in the physically nonexistent, 'ghost' space, with values set to 0, and equal T values on each side from the ghost area.

diagonally. Such a B-grid arrangement with an E-grid definition of the schemes was introduced in Janjić (1984). The scalar points of the B-grid are placed along the boundaries between the tiles. This choice reduces the errors of the pressure gradient force across the boundaries of the faces of the cube and between two back-to-back octagons that comprise the octagonal grid, as pointed out by Rančić *et al.* (1996). The values of the variables in the 'halo' of a tile are acquired by communications from the adjacent tiles. Note that a tile that contains a singular point does not have a neighbouring tile in the diagonal direction.

Just as in the regional Eta model, the variables are vertically staggered using a Lorenz distribution, with the temperature and momentum components defined in the middle of the layers, and the geopotential and the vertical velocity on the interfaces between the layers.

(*b*) *The dynamics*

The equations describing the dynamics of the hydrostatic atmosphere (momentum, thermodynamic, continuity, surface pressure and hydrostatic) are discretized in space as:

$$\frac{\partial u}{\partial t} = \frac{2}{3}\overline{Z}^{x'y'}V + \frac{1}{3}\overline{Z\overline{V}^{y}}^{x} + fG\tilde{v} - \delta_x\overline{K}^{x'y'} - \delta_x\overline{\Phi}^{\eta} - \overline{\pi}^{x}\delta_x\overline{\ln^2 p}^{\eta} - \overline{\dot{\eta}^{x'y'}\delta_\eta u}^{\eta} \quad , (17)$$

$$\frac{\partial v}{\partial t} = -\frac{2}{3}\overline{Z}^{x'y'}U - \frac{1}{3}\overline{Z\overline{U}^{x}}^{y} - fG\tilde{u} - \delta_y\overline{K}^{x'y'} - \delta_y\overline{\Phi}^{\eta} - \overline{\pi}^{y}\delta_y\overline{\ln^2 p}^{\eta} - \overline{\dot{\eta}^{x'y'}\delta_\eta v}^{\eta} \quad ,(18)$$

$$\frac{\partial T}{\partial t} = -\frac{1}{mG}\left(\overline{U\delta_x T}^{x} + \overline{V\delta_y T}^{y}\right) - \overline{\dot{\eta}\delta_\eta T}^{\eta} + \frac{1}{c_p mG}\left(U\overline{\pi}^{x}\delta_x\overline{\ln^2 p}^{\eta} + V\overline{\pi}^{y}\delta_y\overline{\ln^2 p}^{\eta}\right) - \frac{1}{c_p}\overline{\sum_{l'=1}^{l} D_{l'}}^{\eta}\,, \tag{19}$$

$$\frac{\partial m}{\partial t} = -D - \delta_\eta(\dot{\eta} m q)\,, \tag{20}$$

$$\frac{\partial p_s}{\partial t} = -\sum_{l=1}^{l_m} D_l\,, \tag{21}$$

$$\Delta_\eta \Phi = -RT_v \Delta_\eta \ln p\,. \tag{22}$$

The nonlinear advection terms in the momentum equation are discretized using the Janjić (1977) Arakawa-type scheme. A second-order mass and energy conserving spatial differencing is applied for the remaining terms.

The horizontal fluxes, U and V, the relative vorticity, ζ, and the horizontal divergence, D, are defined respectively as

$$U = \overline{mG}^{x'y'}\tilde{u}\,, \qquad V = \overline{mG}^{x'y'}\tilde{v}\,, \tag{23}$$

$$\zeta = \frac{1}{G}(\delta_x v - \delta_y u)\,, \tag{24}$$

$$D = \frac{1}{G}(\delta_x U + \delta_y V)\,. \tag{25}$$

The potential relative vorticity, Z, is defined as:

$$Z = \frac{\zeta}{m}\,. \tag{26}$$

In these expressions, the mass m is defined as the thickness of the *eta* layers $\Delta_\eta p$, and π is:

$$\pi = \frac{RT_v}{2\overline{\ln p}^{\eta}}\,. \tag{27}$$

The operators δ_s and $\overline{(\ )}^{s}$ represent respectively the two-grid-point finite-difference, and an averaging in the s direction.

A standard technique for suppressing the two-grid-interval noise on the semi-staggered grid (Mesinger 1973; Janjić 1979) is adjusted to the curvilinear frame. This technique consists of a modification of the continuity equation, in which a term proportional to

$$-(\nabla_\times \cdot \mathbf{P}' - \nabla_+ \cdot \mathbf{P})$$

is added to the divergence term. Here, $\nabla_\times \cdot$ and $\nabla_+ \cdot$ are the finite-difference analogies of the divergence, and $\mathbf{P}'$ and $\mathbf{P}$ are approximations of the pressure gradient

force calculated in the direction of (x', y') and (x, y) axes, respectively. Using the finite-difference formalism of the general curvilinear system, the modification term may be written as

$$-\frac{1}{G}\{[\delta_{x'}(G\tilde{P_{x'}}) - \delta_{y'}(G\tilde{P_{y'}})] - [\delta_x(G\tilde{P_x}) - \delta_y(G\tilde{P_y})]\} .$$

Here, $\tilde{P_{x'}}$,$\tilde{P_{y'}}$,$\tilde{P_x}$ and $\tilde{P_y}$ are the contravariant components of the pressure gradient force in the corresponding directions. The contravariant components in the diagonal directions, $\tilde{P_x}$ and $\tilde{P_y}$, are:

$$\begin{pmatrix} \tilde{P_x} \\ \tilde{P_y} \end{pmatrix} = \mathbf{G^{-1}} \begin{pmatrix} P_x \\ P_y \end{pmatrix} . \tag{28}$$

In these expressions P_x and P_y are covariant components of the pressure gradient force in x and y direction, respectively, defined as

$$\begin{aligned} P_x &= -\delta_x \overline{\Phi}^{\eta} - \overline{\frac{RT_v}{2\ln p}}^{x} \delta_x \overline{\ln^2 p}^{\eta} , \\ P_y &= -\delta_y \overline{\Phi}^{\eta} - \overline{\frac{RT_v}{2\ln p}}^{y} \delta_y \overline{\ln^2 p}^{\eta} . \end{aligned} \tag{29}$$

The contravariant components in the normal directions, $\tilde{P_{x'}}$ and $\tilde{P_{y'}}$, are similarly defined.

A scalar point located at a corner of the cube or the octagon is surrounded by only three velocity points. In the code, we treat the corner points equally as all other points in the domain, by constructing an artificial 'ghost' space at the place of missing area and by setting the values there to zero. This technique is formally equivalent to a consistent finite-volume reformulation of the vector operators at the corner points, and, as stated in Rančić *et al.* (1996), it enables conservation of the mass, the total energy and the relative vorticity of the general flow (but not the enstrophy of the non-divergent part of the flow).

The model employs the same explicit time-split differencing for the propagation in time as the regional Eta model, with the *adjustment* time-step being half of that applied to the advection processes. The forward-backward scheme is applied to the gravity-wave terms and the trapezoidal implicit scheme to the Coriolis terms (Mesinger 1977; Janjić 1979). Instead of updating the continuity equation with the forward and the momentum equation with the backward time-differencing scheme, as it is done in the regional Eta model, we reverse their order and apply the forward scheme to the momentum and the backward to the continuity equation, which we found to be more accurate (Rančić and Zhang 2002). The same pattern of time-differencing for the adjustment terms is now being tested within the regional Eta model (e.g., Mesinger et al. 2006).

The multidimensional positive-definite flux corrector scheme of Smolarkiewicz and Grabowski (1990) is applied for the horizontal advection of water vapour and cloud water. Vertical advection is computed using unmodified schemes from the regional Eta model: a piecewise linear upstream scheme for the vertical advection of humidity and cloud water and the Euler-backward time scheme for the vertical advection of momentum, temperature, and turbulent kinetic energy.

(*c*) *The physical parameterization*

A comprehensive physical package of the regional Eta model is implemented within the global Eta framework with the minimum modifications.

For parameterization of radiation, the model uses the Geophysical Fluid Dynamics Laboratory (GFDL) scheme (Fels and Schwarzkopf 1975; Lacis and Hansen 1974). The surface soil temperature and moisture are predicted using the land-surface scheme described in Chen *et al.* (1997). The sea surface temperature is prescribed from NCEP analysis and kept constant during integrations in our experiments. The cloud water and ice are treated explicitly as the prognostic variables using the scheme developed by Zhao and Carr (1997). Just like in the regional Eta model, two schemes for cumulus convection are optionally available: BMJ scheme (Betts 1986; Betts and Miller 1986; Janjić 1990) and Kain-Fritsch scheme (Fritsch and Chappell 1980; Kain and Fritsch 1990).

The most notable departures from the physics of the regional Eta model are in the formulation of the horizontal and the vertical diffusion, though the same explicit scheme for propagation in time is applied as in the Eta model.

(*c*).1 **Horizontal diffusion**

The fourth-order scheme for the lateral diffusion, which is more scale selective than the second-order scheme and less affects the larger scales, is applied at the adjustment time-steps for temperature, turbulent kinetic energy and momentum field.

The diffusion is expressed by a fourth-order Laplacian operator applied in the normal x' and y' directions where the grid distance is minimal. Instead of using the general curvilinear system, we approximate the Laplacian operator using a conformal formalism. Technically, we define a new local conformal coordinate system (and a new corresponding stencil of grid points) centred at the point to which we apply the diffusion operator. The values of the variable at the points of the local stencil are derived by the high-order interpolations from the model variables. When applying diffusion to the momentum, we additionally need to project winds to the base vectors of the local stencil, and then the resulting Laplacian back to base general curvilinear coordinates, in order to get its covariant components.

This method is designed to cope with the problems that otherwise may arise due to a combined effect of a strong curvature of the coordinate lines close to the corners and the application of the fourth-order operator for diffusion, which uses spatially rather distant grid points.

(*c*).2 **Vertical diffusion**

Vertical diffusion is applied every 6 adjustment steps to temperature, momentum, water vapour and turbulent kinetic energy. The diffusion coefficients are obtained from the turbulent closure schemes described in Janjić (1990; 1994).

Similarly as in the case of horizontal diffusion, we design an interface for transformation between the covariant wind components of the curvilinear system and a locally orthogonal system defined at each scalar point separately. Through this interface, the turbulence module from the regional Eta model, which assumes vertical profiles of the orthogonal wind components, is directly, without modifications, applied to the global Eta model.

4. Results

In this section we present the results of several test integrations of the developed global modelling framework. The dry dynamical core is tested in the traditional benchmark test of Held and Suarez (1994). The model with full physics is run in a series of 10-day integrations using real data.

(*a*) *Held-Suarez test*

The Held-Suarez test (HS94 hereafter) is commonly used for verification of the dynamical cores of atmospheric models. In this test, the temperature field is relaxed to a prescribed zonally symmetric equilibrium state using a Rayleigh damping at the low-level winds to represent the boundary layer friction.

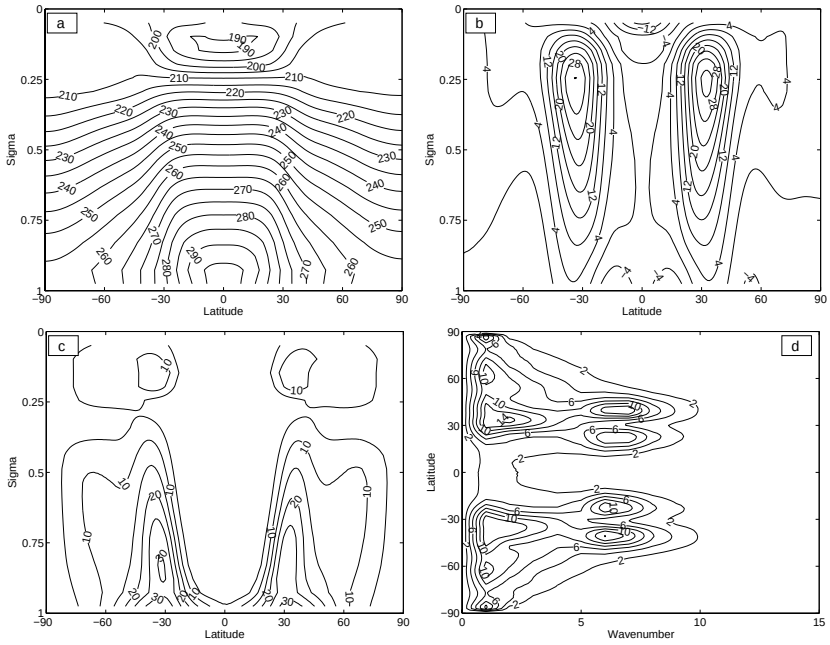

Figure 3. HS94 test of the C42 cubic grid. (a) Zonal mean temperature; (b) Zonal mean wind; (c) Zonal mean zonal wind; (d) Zonal-time mean temperature eddy variance.

Both cubic and octagonal grid models have been integrated in this test with the fairly similar outcome. Therefore, only the results with the cubic grid will be presented here for brevity.

The horizontal resolutions of the cubic grid model is set to C42 ($42 \times 42 \times 6$ grid boxes). Here, the 'grid box' is defined as a five-point stencil on the B-grid with the wind point in the middle and four scalar points at the corners. The vertical resolution has 20 layers and the pressure at the top of the atmosphere is 25 mb. The model starts integration from an isothermal atmosphere at rest and integrates for 1200 days. The statistics are computed for the last 1000 days. The forth-order horizontal diffusion, applied to the temperature and wind field, simulates the physics.

Figures 3 present fields that are obtained in these simulations. These results generally agree with the solution suggested as the reference in HS94. Figure 3 a

and Figure 3 b show the zonally averaged temperature and the zonally averaged zonal wind, respectively. The midlatitude jets are located at about 40° latitude with the strength of about 30 m/s. The surface maximum westerlies are about 4 m/s. The model produces tropical easterlies at all levels. Compared with the results from HS94, the midlatitude jets are shifted slightly toward equator, and the surface wind is somewhat weaker.

The eddy temperature variance is shown in Figure 3 c. Two maxima are formed in the midlatitude, one in the lower troposphere and another above the tropopause. The zonal spectrum of the vertically averaged zonal wind variance is shown in Figure 3 d. The peaks are at the same location as in the HS94, with slightly smaller intensity, and the two midlatitude maxima are at the wavenumber six rather than at the wavenumber five.

In order to investigate convergence of the derived solution (e.g., Ringler et al. 2000), additional test with the cubic grid at a high resolution (C84, 84x84x6 grid boxes) is also performed. The results, shown in Figure 4, are closer to those suggested as the reference in HS94. The midlatitude easterlies are located at 45°, the temperature eddy variance is larger than in C42 experiment, and the two maxima of midlatitude zonal wind spectra are located at the wavenumber five.

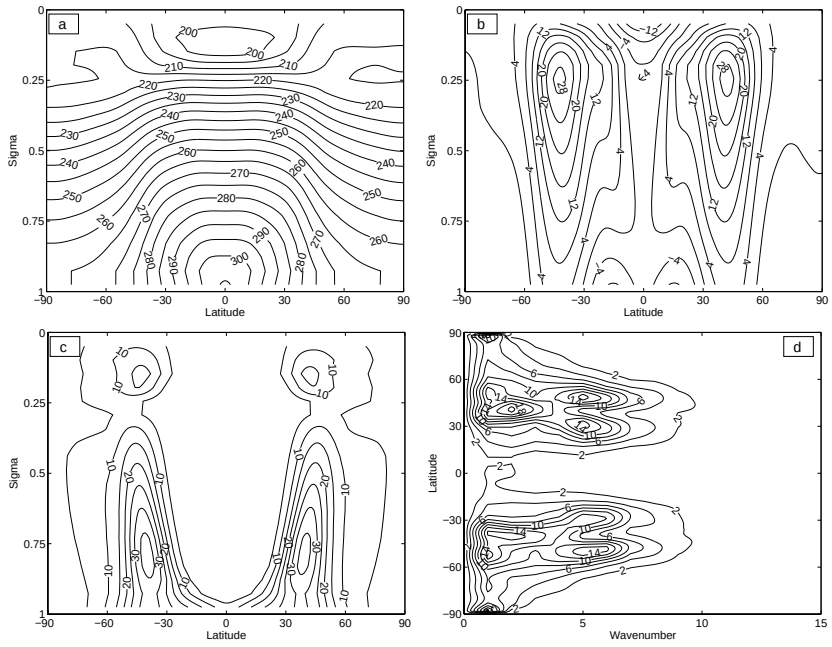

Figure 4. HS94 test of the C84 cubic grid. (a) Zonal mean temperature; (b) Zonal mean wind; (c) Zonal mean zonal wind; (d) Zonal-time mean temperature eddy variance.

(*b*) *Tests with real data*

The developed model is tested in integrations with full physics using real data, on both the cubic and the octagonal grid. The average horizontal grid distance used in these tests is shown in Table 1. The corresponding horizontal resolutions,

model	grid distance (km)	resolution	# of grid boxes
C42	219	$42 \times 42 \times 6$	10584
C100	92	$100 \times 100 \times 6$	60000
C200	46	$200 \times 200 \times 6$	240000
O28	215	$28 \times 28 \times 14$	10976
O68	89	$68 \times 68 \times 14$	64736
O134	45	$134 \times 134 \times 14$	251384

TABLE 1. Grid resolutions in the tests with real data.

expressed as the number of wind points, are also summarized in Table 1. The number of scalar points can be obtained using a general formula:

$$N_s = \tau n^2 + 2 \,, \tag{30}$$

where τ is the number of basic grid elements (6 for cubic and 14 for octagonal grid), and n is the number of wind grid boxes in each dimension of such an element.

The vertical resolution has 38 levels, which is a predefined number of levels in the regional Eta model, structured with a higher density close to the surface. The pressure at the top of the atmosphere is 25 mb.

In these integrations, the primary three-dimensional atmospheric fields, soil moisture and sea surface temperature are interpolated from the NCEP's global analysis, available at one degree of horizontal resolution. The snow cover in the North Hemisphere is determined from the 47-km U.S. Air Force global snow depth analysis and the 23-km daily NESDIS (National Environmental Satellite, Data and Information Service) Northern Hemisphere snow cover analysis. In the Southern Hemisphere, the snow cover was determined from NCEP global analysis data. The initial albedo is derived by interpolation from the seasonal climate values.

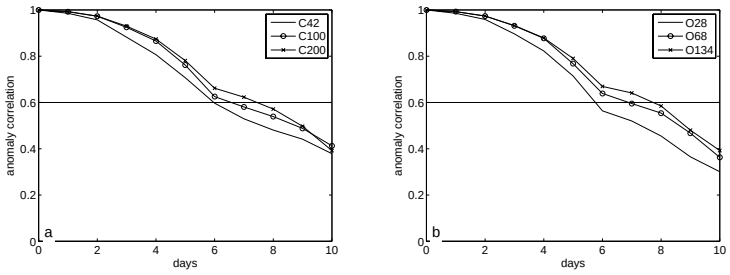

Figure 5. Anomaly correlation of the forecasted 500 mb height with analysis, calculated for the Northern Hemisphere in region of $20^\circ - 80^\circ N$: cubic grid (left); octagonal grid (right).

(b).1 **Convergence in the tests with real data**

Two randomly selected 10-day test cases are run over the whole span of chosen horizontal resolutions. The initial conditions are taken from 1 February 2005

(Case 1) and 10 March 2005 (Case 2), respectively, both at 0000 UTC (Coordinated Universal Time). The anomaly correlation coefficient of 500 mb height for the Northern Hemisphere in the region from 20° to 80° is computed every 24 h for 10 days. The averaged values for these two test cases for different resolutions and both grids are drawn in Figure 5.

The forecasting skill of 500 mb surface increases steadily with the increase of horizontal resolution, though more significantly in the transition from about 200 km to about 100 km, than from about 100 km to about 50 km.

These results compare favourably against the results that Wyman (1996) derived using a global version of the Eta model on the longitude-latitude grid with resolutions E45 (with 5342 grid points) and E60 (with 9522 grid points), both with 18 vertical levels.

As an illustration, Figures 6 show 500 mb height in the polar stereographic projection of the North Hemisphere for the Case 2 after 5 days of integration on both grids (models C100 and O68), along with the analysis. Both forecasts compare well with the analysis, showing some minor differences. These differences in the model performance between two different grids, as well as the departure from the analysis, steadily grow, and become quite evident after day 10.

(*b*).2 Comparison with the regional Eta model

One of the expected benefits of a global model is that it does not have to deal with the lateral boundary conditions and the related problems of the limited-area models. The regional Eta model has an efficient method for dealing with the lateral boundaries (e.g., Mesinger 2000). Yet, we expect that as the integration time increases, the errors will still develop near the boundaries and gradually affect the performance of the regional model. In order to verify this hypothesis, the regional Eta model was run at 48 km for both selected cases, with the lateral boundary conditions taken form the NCEP's Global Forecasting System. The average anomaly correlation is calculated for a domain covering the continental United States and the surrounding seas, that as, a box between $25 - 50°$ North, and $66 - 126°$ West, and compared against the correlation of the global models on the cubic and the octagonal grid (Figure 7), respectively, which are integrated at similar grid resolutions (C200 and O134). After first three days, the difference between the regional and global models becomes noticeable. Since the global models have a similar dynamics and the same physics as the regional model, we assume that the weaker performance of the regional Eta model during day 4 and 5 is caused by the effects of boundary conditions. It is more surprising, however, that the regional model regains its skill relative to the global models between days 6 to 8. However, similar capability of the regional Eta model to maintain the forecasting skill in longer time integrations has been already observed in past(e.g., Mesinger 2004).

(*b*).3 Comparison of cubic and octagonal grids

In order to preliminary compare the model performance on the cubic and the octagonal grid with some statistical significance, we run ten additional 10-day integrations for February 2005 at a moderate resolution, with models C100 and O68. The integrations start at 0000 UTC every other day beginning with February 2, 2005. The average 500 mb anomaly correlation and the standard deviation

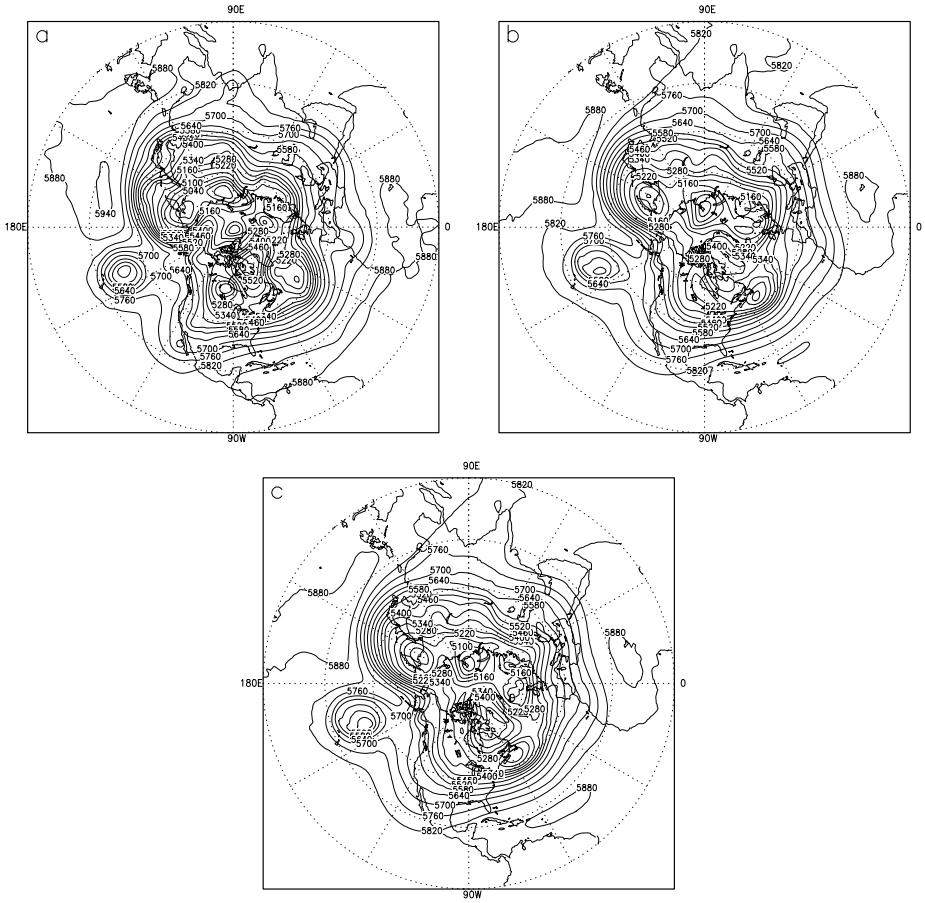

Figure 6. North Hemisphere 500-mb height at 0000 UTC 15 March 2005 (a) analysis (b) cubic grid (c) octagonal grid.

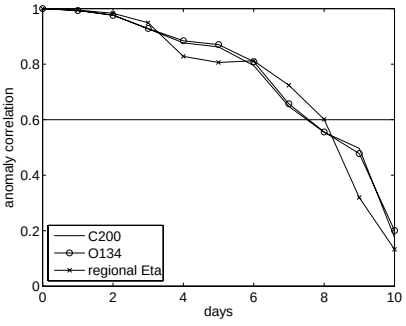

Figure 7. Anomaly correlation of 500 mb height over the United States area for the global Eta model on cubic and octagonal grid, and for the regional Eta model, respectively.

are presented in (Table 2 and Table 3). The two models have a very similar performance in these tests, though the model on the cubic grid performs slightly better than the model on the octagonal grid.

day	1	2	3	4	5	6	7	8	9	10
C100	0.987	0.962	0.921	0.858	0.780	0.697	0.615	0.544	0.479	0.382
O68	0.987	0.962	0.921	0.855	0.774	0.689	0.612	0.539	0.464	0.369

TABLE 2. Average 500 mb anomaly correlation in a series of ten additional integrations

day	1	2	3	4	5	6	7	8	9	10
C100	0.0019	0.0063	0.015	0.029	0.037	0.048	0.049	0.078	0.12	0.13
O68	0.0019	0.0067	0.016	0.031	0.040	0.048	0.053	0.081	0.13	0.14

TABLE 3. Standard deviation of 500 mb anomaly correlation in a series of ten additional integrations

(*c*) *Computational efficiency*

The major motivation for application of the quasi-uniform grids is their clear potential for improving the computational efficiency. The quasi-uniform grid topology enables a balanced distribution of the computational load across the processors of the massively parallel computer, so that each processor is engaged with the maximum of its efficiency.

In order to demonstrate this feature of the developed modelling framework, we compare the computational efficiency of dry core of GEF against a model that exploits the standard longitude-latitude grid. For this comparison, we use a B-grid version of the atmospheric dynamical core of a Flexible Modeling System (FMS), developed by a GFDL Modeling Team (2004). This is a grid-point model on the longitude-latitude grid which relies on the application of Fourier polar filtering. The dynamical cores of two models are compared on an IBM 1350 Beowulf Linux cluster with the high performance capability.

The FMS has horizontal resolution of $144 \times 72 \times 20$, which corresponds to 10368 grid-points. GEF is run at horizontal grid configurations C42 and O28 (see Table 1 for the corresponding horizontal resolutions). Both models have 20 vertical layers.

Table 4 shows the results of the comparison with different number of processors. The time-steps are set at the maximum values capable to maintain a stable integration, which in this case are 360 s, 430 s and 355 s for C42, O28 and FMS model, respectively. In spite of application of the Fourier filtering (from standard 60 $^\circ$ of latitude toward poles), the time-step of FMS is still smaller than that of the global Eta models. The Fourier filtering in these tests takes about 20% of total run time of the FMS model. Consequently, the global model on the quasi-uniform grids, performs more efficiently than the global model on the longitude-latitude grid.

model	time step (sec)	# of processors	Run time per simulated day (sec)	Time spent on polar filtering per simulated day (sec)
C42	360	6	24.0	0
C42	360	24	8.0	0
O28	430	14	10.1	0
FMS	355	6	50.6	10.6
FMS	355	14	26.8	6.8
FMS	355	24	14.9	3.0

TABLE 4. Comparison of efficiency of GEF and FMS model

5. Conclusions

Quasi-uniform grids eliminate the necessity for polar filtering and generally promise to improve the computational efficiency. A global version of the regional Eta model has been developed on the quasi-uniform cubic and octagonal grids.

The model dynamics is formulated in terms of general curvilinear system, so that the only difference between the models on the cubic and the octagonal grid (as well as on any other quasi-uniform grid with the rectangular base elements) is in formulation of communications between the processing elements. The physical parameterization is taken from the regional Eta model with the minimum modifications. The model can be used both for weather forecasting and climate simulations, and represents a pioneering prototype for a quasi-uniform expansion of the regional models of the atmosphere to global coverage.

The dry core of the new model is successfully tested in the Held-Suarez tests. The model performance with full physics is verified in a series of 10 days integrations at different resolutions. Both grids give similar forecasts of 500 mb surface, with the model on the cubic grid being slightly better than the model on the octagonal grid, presumably because of the higher resolution in the extratropical regions. However, note from Table 4 that the octagonal grid is capable of supporting the larger time-steps than the cubic grid. Over the United States, the diagnostics of the anomaly correlation of the 500 mb height is compared to that derived in the corresponding integrations of the regional Eta model. After three days of integration, the global models are clearly better as expected, though after day 7 the regional model starts regaining its relative skill for a while, among other reasons, most likely because of a somewhat better nonlinear momentum advection scheme. Generally, the global model on the quasi-uniform grids performs better than a global version of the Eta model on the longitude-latitude grid (Wyman 1996). Dynamical cores of both developed versions of the global Eta model are more efficient than the corresponding dynamical core of atmospheric part of the GFDL's Forecasting Modeling System.

Admittedly, the method for treatment of the horizontal diffusion in the curvilinear settings of the global model on the quasi-uniform grids is more time consuming than it would be in the orthogonal frame. For example, the fourth-order horizontal diffusion in the global model takes 13.4% out of time spent on calculation of the dynamical core, and only 10.5% in the regional model.

Work on further testing and improvements of the developed modelling framework is under way.

A more comprehensive testing of various aspects of the model performance, including comparison of the climatology of the cubic, the octagonal and the

longitude-latitude grid versions of the model in the long-term simulations, needs to be done.

One of the strongest features of the regional Eta model is the Janjić (1984) Arakawa type nonlinear advection scheme, as well as its fourth-order counter part (Rančić 1988), which both successfully constrain the flow of energy in the nonlinear cascading toward (or from) the smallest resolvable scales. We expect that the implementation of these schemes will further significantly improve the performance of the presented modelling framework.

Another direction of development is the inclusion of the variable resolution using the method of grid stretching (e.g., Fox-Rabinovitz *et al.* 2001) and application for the regional climate downscaling. We have recently finished preliminary testing of the variable resolution concept in the context of quasi-uniform grids (Rančić and Zhang 2006) and we now start working on implementations of grid stretching in the model with full physics.

A version of the regional Eta model with the 'slope' (e.g., Adcroft *et al.* 1997) instead of the 'step' approximation of the terrain is now available (Mesinger and Jović 2004) and incorporation of this upgrade into the global Eta model framework is also one of the future tasks.

Acknowledgement

The U.S. National Science Foundation (Award Number ATM-0113037) and internal founds from Joint Center for Earth Systems Technology (JCET) sponsored the work on this project. We used the Beowulf cluster at the Department of Mathematics and Statistics of the University of Maryland, Baltimore County (UMBC) for numerical integrations, which was partially supported by the SCREMS grant DMS-0215373 from the U.S. National Science Foundation, with additional support from UMBC. The authors are grateful to Dr. Ray Hoff, the Director of JCET for his support. Special thanks to Prof. Matthias Gobbert and Prof. Wallace McMillan from UMBC for their help. We also would like to acknowledge the contribution of unknown reviewers of the first version of the manuscript, whose remarks and comments significantly improved the clarity and level of presentation.

References

Adcroft, A., Hill C., and Marshall, J.	1997	Representation of topography by shaved cells in a height coordinate ocean model. *Mon. Weather Rev.,* **125,** 2293-2315
Arakawa, A. and Lamb, V. R.	1977	Computational design of the basic dynamical processes of the UCLA general circulation model. in *Methods in Computational Physics.* 173-265, Academic Press
Betts, A. K.	1986	A new convective adjustment scheme. Part I: Observational and theoretical basis. *Q. J. R. Meteorol. Soc.,* **112,** 677-691
Betts, A. K. and Miller, M. J.	1986	A new convective adjustment scheme. Part II: single column tests using GATE wave, BOMEX and arctic air-mass data sets. *Q. J. R. Meteorol. Soc.,* **112,** 693-709
Black, T. L.	1994	The new NMC mesoscale Eta model: Description and forecast examples. *Weather and Forecasting,* **9,** 265-278
Browning, G. L., Hack. J. J. and Swarztrauber, P. N.	1989	A comparison of three numerical methods for solving differential equations on the sphere. *Mon. Weather Rev.,* **117,** 1058-1075
Chen, F., Janjić, Z. and Mitchell, K.	1997	Impact of atmospheric surface-layer parameterizations in the new land-surface scheme of the NCEP mesoscale Eta model. *Boundary-Layer Meteorol.,* **85,** 391-421

Ek, M. B., Mitchell, K. E., Lin, Y., Rogers, E., Grunmann, P., Koren, V., Gayno, G. and Tarpley, J. D.	2003	Implementation of Noah land surface model advances in the National Centers for Environmental Prediction operational mesoscale Eta model. *J. Geophys. Res.* **108(D22)** GCP 12-1 - GCP 12-16
Fels, S. B. and Schwarzkopf, M. D.	1975	The simplified exchange approximation: a new method for radiative transfer calculations. *J. Atmos. Sci.,* **32,** 1475-1488
Fox-Rabinovitz, M. S., Takacs, L. L., Govindaraju, R. C. and Suarez, M.	2001	A variable resolution stretched-grid general circulation model: regional climate simulation. *Mon. Weather Rev.,* **129,** 453-469
Fritsch, J. M. and Chappell, C. F.	1980	Numerical prediction of convectively driven mesoscale pressure systems. Part I: convective parameterization. *J. Atmos. Sci.,* **37,** 1722-1733
GFDL Global Atmospheric Model Development Team (list of 33 authors)	2004	The new GFDL global atmospheric and land model. AM2-LM2: Evaluation with prescribed SST simulation. *J. Climate,* **17,** 4641-4673
Held, I. and Suarez, M.	1984	A proposal for intercomparison of the dynamical cores of atmospheric general circulation models. *Bull. Am. Meteorol. Soc.,***73,** 1825-1830.
Janjić, Z. I.	1977	Pressure gradient force and advection scheme used for forecasting with steep and small scale topography. *Beitr. Phys. Atmos.,* **50,** 186-199
	1979	Forward-backward scheme modified to prevent two-grid-interval noise and its application in sigma coordinate models. *Beitr. Phys. Atmos.,* **52,** 69-84
	1984	Nonlinear advection schemes and energy cascade on semi-staggered grids. *Mon. Weather Rev.,* **112,** 12341245
	1990	The step-mountain coordinate: physical package. *Mon. Weather Rev.,* **118,** 1429-1443
	1994	The step-mountain eta coordinate model: Further developments of the convection, viscous sublayer, and turbulence closure schemes. *Mon. Weather Rev.,* **122,** 927-945
Kain, J. and Fritsch, J. M.	1990	A one-dimensional entraining/detraining plume model and its application in convective parameterization. *J. Atmos. Sci.,* **47,** 2784-2802
Lacis, A. A. and Hansen, J. E.	1974	A parameterization for the absorption of solar radiation in the earth's atmosphere. *J. Atmos. Sci.,* **31,** 118-133
McGregor, J. L.	1996	Semi-Lagrangian advection on conformal-cubic grids. *Mon. Weather Rev.,* **124,** 1311-1322
McGregor, J.L. and Dix, M. R.	2001	The CSIRO conformal-cubic atmospheric GCM. In *IUTAM Symposium on Advances in Mathematical Modelling of Atmosphere and Ocean Dynamics,* Ed. P. F. Hodnett, Kluwer, Dordrecht, 197-202
Mesinger, F.	1973	A method for construction of second-order accuracy difference schemes permitting no false two-grid-interval wave in the height field. *Tellus,* **25,** 444-458
	1977	Forward-backward scheme, and its use in a limited area model. *Beitr. Phys. Atmos.,* **50,** 200-210
	1984	A blocking technique for representation of mountains in atmospheric models. *Riv. Meteor. Aeronautica.,* **44,** 195-202
	1996	Improvements in quantitative precipitation forecasts with the Eta regional model at the National Centers for Environmental Prediction. The 48-km upgrade. *Bull. Am. Meteorol. Soc.,* **77,** 2637-2649
	2000	Numerical Methods: The Arakawa approach, horizontal grid, global and limited-area modeling. In: *General Circulation Model Development. Past, Present and Future.* Academic Press, Ed. D. A. Randall, 373-419
	2004	Dynamical core design: A neglected thrust toward increasing NWP skill several days ahead. In: *The First THORPEX International Science Symposium.* Montreal, Canada, 6-10 December 2004

Mesinger, F., and Janjić, Z. I. 1985 Problems and numerical methods of the incorporation of mountains in atmospheric models. In *Large-scale Computations in Fluid Mechnaics,* Part 2, *Lect. Appl. Math.,* **22,** 81-120

Mesinger, F., Janjić, Z. I., Ničković, S., Gavrilov, D. and Deaven, D. G. 1988 The step mountain coordinate: Model description and performance for cases of Alpine Cyclogenesis and for a case of an Appalachian redevelopment. *Mon. Weather Rev.,* **116,** 1493-1518

Mesinger, F., Black, T., Brill, K., Chuang, H.-Y., DiMego, G. and Rogers, E. 2002 A decade+ of the Eta performance, including that beyond two days: Any lessons for the road ahead? *Preprints, 19th Conf. on Weather Analysis and Forecasting/15th Conf. on Numerical Weather Prediction,* San Antonio, TX, Am. Meteorol. Soc., 387-390

Mesinger, F. and Jović, D. 2004 Vertical coordinate, QPF, and resolution. *The 2004 Workshop on the Solution of Partial Differential Equations on the Sphere, Frontier Res. Center for Global Change (FRCGC),* Yokohama, Japan, 20-23 July 2004. ppt in CD-ROM, Vol. 2. Available also at http://www.jamstec.go.jp/frcgc/eng/workshop/pde2004/agenda.html.

Mesinger, F., Rančić, M., Jović, D., Zhang. H., and Popović, J. 2006 Forward-backward scheme modified to suppress lattice separation and impact of the order of execution. General Assembly of the European Geosciences Union, Vienna, Austria, Vienna, Austria, 02 - 07 April 2006, EGU06-A-10164.

Phillips, N. A. 1957 A coordinate system having some special advantages for numerical forecasting. *J. Meteorol.,* **14,** 184-185

1959 Numerical integration of the primitive equations on the hemisphere. *Mon. Weather Rev.,* **87,** 333-345

Purser, R.J. and Rančić, M. 1997 Conformal octagon: an attractive framework for global models offering quasi-uniform regional enhancement of resolution. *Meteorol. Atmos. Phys.,* **62,** 33-48

1998 Smooth quasi-homogeneous gridding of the sphere. *Q. J. R. Meteorol. Soc.,* **124,** 637-647

Rančić, M., 1988 Fourth-order horizontal advection schemes on the semi-staggered grid. *Mon. Weather Rev.,* **116,** 1274-1288

Rančić, M. and Ničković, S. 1988 Numerical testing of E-grid horizontal advection schemes on the hemisphere. *Beitr. Phys. Atmos.,* **61,** 265-274

Rančić, M., Purser, R.J. and Mesinger, F. 1996 A global shallow-water model using an expanded spherical cube: gnomonic versus conformal coordinates. *Q. J. R. Meteorol. Soc.,* **122,** 959-982

Rančić, M., and Zhang, H. 2002 A framework for globalization of regional atmospheric models: Dry core and quasi-uniform grids. In: *Preprints, 15th Conference of Numerical Weather Prediction.* San Antonio, Texas, 12-16 August 2002. American Meteorological Society. 4B6

2006 Variable resolution on quasi-uniform grids: Linear advection experiments. *Meteorol. Atmos. Phys.,* DOI 10.1007/s00703-005-0165-4

Ringler, T., Heiks, R. P., Randall, D. 2000 Modeling the atmospheric general circulation using a spherical geodesic grid: A new class of dynamical cores. *Mon. Weather Rev.,* **128,** 2471-2489

Ringler, T. and Randall, D. 2002 Potential enstrophy and energy conserving numerical scheme for solution of the shallow water equations on a geodesic grid. *Mon. Weather Rev.,* **130,** 1397-1410

Ronchi, C., Iaccono, R., Paolucci, P. S. 1996 The 'cubed sphere': A new method for the solution of partial differential equations in spherical geometry. *J. Comput. Phys.,* **124,** 93-114

Sadourny, R. 1972 Conservative finite-differencing approximations of the primitive equations on quasi-uniform spherical grids. *Mon. Weather Rev.,* **22,** 1107-1115

Sadourny, R., Arakawa, A. and Mintz, Y. 1968 Integration of the nondivergent barotropic vorticity equation with an icosahedral-hexagonal grid for the sphere. *Mon. Weather Rev.,* **96,** 351-356

Smolarkiewicz, P. K. and Grabowski, W. W. 1990 The multidimensional positive definite advection transport algorithm: nonoscillatory option. *J. Comput. Phys.,* **86,** 355-375

Tsugawa, M., Tanaka, Y., Mimura, Y., and Sakashita, M. 2003 Approach to a high-resolution parallel OGCM for the Earth Simulator. *The 5th International Workshop on Next Generation Climate Models for Advanced High Performance Computing Facilities,* March 3-5, 2003 at INGV in Rome, Italy

Warner, T. T., Peterson, R. A. and Treadon, R. T. 1997 A tutorial on lateral boundary conditions as a basic and potentially serious limitation to regional numerical weather prediction. *Bull. Am. Meteorol. Soc.,* **78,** 2599-2617

Wayman, B. L. 1996 A step-mountain coordinate general circulation mode: Description and validation of medium-range forecasts. *Mon. Weather Rev.,* **124,** 102-121

Williamson, D. L. 1970 Integration of the primitive barotropic model over a spherical geodesic grid. *Mon. Weather Rev.,* **98,** 512-520

Zhao, Q. and Carr, F. H. 1997 A prognostic cloud scheme for operational NWP models. *Mon. Weather Rev.,* **125,** 1931-1953